APPENDIX I

Double-barred matrices of the trigonal field $(\alpha S\Gamma\|V(T_2)\|\alpha' S\Gamma')$ within the $t_2^4e^4$, $t_2^5e^3$, and $t_2^6e^2$ configurations. Unlisted matrices are zero. K' and K are defined in Eqs. (3b) and (3a), respectively.

$\alpha S\Gamma$	$\alpha' S\Gamma'$	The values
$t_2^6e^2\ ^3A_2$	$t_2^5e^3\ ^3T_1$	$2\sqrt{3}K'$
$t_2^6e^2\ ^1E$	$t_2^5e^3\ ^1T_1$	$2\sqrt{3}K'$
$t_2^6e^2\ ^1E$	$t_2^5e^3\ ^1T_2$	$-2\sqrt{3}K'$
$t_2^6e^2\ ^1A_1$	$t_2^5e^3\ ^1T_2$	$2\sqrt{3}K'$
$t_2^5e^3\ ^3T_2$	$t_2^5e^3\ ^3T_2$	$-\frac{3}{2}\sqrt{2}K$
$t_2^5e^3\ ^3T_2$	$t_2^5e^3\ ^3T_1$	$\frac{3}{2}(\sqrt{6})K$
$t_2^5e^3\ ^3T_2$	$t_2^4e^4\ ^3T_1$	$-2(\sqrt{6})K'$
$t_2^5e^3\ ^3T_1$	$t_2^5e^3\ ^3T_1$	$-\frac{3}{2}\sqrt{2}K$
$t_2^5e^3\ ^3T_1$	$t_2^4e^4\ ^3T_1$	$6\sqrt{2}K'$
$t_2^5e^3\ ^1T_2$	$t_2^5e^3\ ^1T_2$	$-\frac{3}{2}\sqrt{2}K$
$t_2^5e^3\ ^1T_2$	$t_2^5e^3\ ^1T_1$	$\frac{3}{2}(\sqrt{6})K$
$t_2^5e^3\ ^1T_2$	$t_2^4e^4\ ^1T_2$	$-2(\sqrt{6})K'$
$t_2^5e^3\ ^1T_2$	$t_2^4e^4\ ^1E$	$8K'$
$t_2^5e^3\ ^1T_2$	$t_2^4e^4\ ^1A_1$	$-4\sqrt{2}K'$
$t_2^5e^3\ ^1T_1$	$t_2^5e^3\ ^1T_1$	$-\frac{3}{2}\sqrt{2}K$
$t_2^5e^3\ ^1T_1$	$t_2^4e^4\ ^1T_2$	$-6\sqrt{2}K'$
$t_2^4e^4\ ^3T_1$	$t_2^4e^4\ ^3T_1$	$-3\sqrt{2}K$
$t_2^4e^4\ ^1T_2$	$t_2^4e^4\ ^1T_2$	$3\sqrt{2}K$
$t_2^4e^4\ ^1T_2$	$t_2^4e^4\ ^1E$	$-2\sqrt{3}K$
$t_2^4e^4\ ^1T_2$	$t_2^4e^4\ ^1A_1$	$2(\sqrt{6})K$

APPENDIX II

Double-barred matrices of the orbital angular momentum $(\alpha S\Gamma\|L\|\alpha' S\Gamma')$ within the $t_2^4e^4$, $t_2^5e^3$ and $t_2^6e^2$ configurations. Unlisted matrices are zero. k' and k are defined in Eqs. (9d) and (9c), respectively.

$\alpha S\Gamma$	$\alpha' S\Gamma'$	The values
$t_2^6e^2\ ^3A_2$	$t_2^5e^3\ ^3T_2$	$2\sqrt{3}ik'$
$t_2^6e^2\ ^1E$	$t_2^5e^3\ ^1T_1$	$-2\sqrt{2}ik'$
$t_2^6e^2\ ^1E$	$t_2^5e^3\ ^1T_2$	$2\sqrt{2}ik'$
$t_2^6e^2\ ^1A_1$	$t_2^5e^3\ ^1T_1$	$2\sqrt{3}ik'$
$t_2^5e^3\ ^3T_2$	$t_2^5e^3\ ^3T_2$	$-\frac{1}{2}(\sqrt{6})ik$
$t_2^5e^3\ ^3T_2$	$t_2^5e^3\ ^3T_1$	$\frac{3}{2}\sqrt{2}ik$
$t_2^5e^3\ ^3T_2$	$t_2^4e^4\ ^3T_1$	$-6\sqrt{2}ik'$
$t_2^5e^3\ ^3T_1$	$t_2^5e^3\ ^3T_1$	$\frac{1}{2}(\sqrt{6})ik$
$t_2^5e^3\ ^3T_1$	$t_2^4e^4\ ^3T_1$	$2(\sqrt{6})ik'$
$t_2^5e^3\ ^1T_2$	$t_2^5e^3\ ^1T_2$	$-\frac{1}{2}(\sqrt{6})ik$
$t_2^5e^3\ ^1T_2$	$t_2^4e^4\ ^1T_2$	$-6\sqrt{2}ik'$
$t_2^5e^3\ ^1T_2$	$t_2^5e^3\ ^1T_1$	$\frac{3}{2}\sqrt{2}ik$
$t_2^5e^3\ ^1T_2$	$t_2^4e^4\ ^1T_2$	$-6\sqrt{2}ik'$
$t_2^5e^3\ ^1T_1$	$t_2^5e^3\ ^1T_1$	$\frac{1}{2}(\sqrt{6})ik$
$t_2^5e^3\ ^1T_1$	$t_2^4e^4\ ^1T_2$	$2(\sqrt{6})ik'$
$t_2^5e^3\ ^1T_1$	$t_2^4e^4\ ^1E$	$-8ik'$
$t_2^5e^3\ ^1T_1$	$t_2^6e^4\ ^1A_1$	$-2\sqrt{2}ik'$
$t_2^4e^4\ ^3T_1$	$t_2^4e^4\ ^3T_1$	$-(\sqrt{6})ik$
$t_2^4e^4\ ^1T_2$	$t_2^4e^4\ ^1T_2$	$-(\sqrt{6})ik$
$t_2^4e^4\ ^1T_2$	$t_2^4e^4\ ^1E$	$2\sqrt{3}ik$

PHYSICAL REVIEW VOLUME 128, NUMBER 3 NOVEMBER 1, 1962

Magnetothermal Oscillations. The Oscillatory Dependence of Temperature on Magnetic Field

J. E. KUNZLER, F. S. L. HSU, AND W. S. BOYLE*
Bell Telephone Laboratories, Murray Hill, New Jersey

(Received June 1, 1962)

Magnetothermal oscillations are a new low-temperature phenomenon. They result from quantum effects and can be employed as a useful tool for exploring the electronic band structure of metals. Magnetothermal oscillations show up experimentally as a reversible and cyclic variation of the temperature of a thermally isolated single crystal, such as bismuth, as either the magnitude or the direction of an externally applied magnetic field is changed in a uniform manner. The oscillatory temperature changes are periodic in $1/H$, and their variation with orientation is dependent on the detailed shape of the pertinent part of the Fermi surface in much the same manner as magnetic susceptibility oscillations. Of the oscillatory effects used for the study of Fermi surface shapes at moderate magnetic fields, magnetothermal oscillations have yielded the best resolution in bismuth. The high resolution obtained in the magnetothermal experiments made it possible to observe for the first time fine structure in de Haas-van Alphen oscillations due to electron spin. Data for bismuth, showing magnetothermal oscillations as a function of magnetic field strength or the field direction, are presented and discussed.

I. INTRODUCTION

EXPERIMENTALLY, magnetothermal oscillations are reversible changes in temperature of a thermally isolated single crystal, such as bismuth, as either the magnitude or direction of an externally applied magnetic field is slowly changed. The observed oscillatory temperature changes are periodic in $1/H$ as the magnitude of the magnetic field is varied while its orientation is fixed.[1–3] However, the relationship between the oscillations observed on changing the magnetic-field direction cannot be defined in such a simple manner. These temperature changes take the form of cooling peaks when the magnitude and orientation are in the

* Present address: Bellcom, Inc., Washington, D. C.

[1] J. E. Kunzler and W. S. Boyle, Bull. Am. Phys. Soc. 4, 168 (1959); J. E. Kunzler, *ibid.* 4, 319 (1959).

[2] W. S. Boyle, F. S. L. Hsu, and J. E. Kunzler, Phys. Rev. Letters 4, 278 (1960).

[3] J. E. Kunzler and F. S. L. Hsu, in *The Fermi Surface*, edited by W. A. Harrison and M. B. Webb (John Wiley & Sons, New York, 1960), p. 88.

proper combination. These peaks are quite sharp for the magnetic field along particular crystal directions. This behavior is a consequence of the fact that the entropy of the conduction electrons in bismuth varies in an oscillatory manner with both the direction and the magnitude of the magnetic field. The crystal lattice is not appreciably affected by a magnetic field, and since the electrons and the lattice are in good thermal contact, any adiabatic variation of the entropy of the electrons must be shared by the lattice. Therefore, with a suitable thermometer in good thermal contact with the sample, the variations in the entropy of the electron system, as the magnetic field is varied in either direction or magnitude, are observed as temperature changes.

The physical origin of this effect is quite closely related to that of the magnetic susceptibility oscillations of the de Hass-van Alphen effect.[4] In the case of the susceptibility, each oscillation is the result of an oscillation in the free energy, whereas the magnetothermal oscillations involve only the entropy or thermal part of the free energy and are thus a direct measure of the change in the density of states at the Fermi surface. Since entropy is the temperature coefficient of free energy, the magnitude of the thermal peaks is thermodynamically related to the temperature coefficient of the susceptibility peaks.

The speed and simplicity with which continuous observations can be made, as a function of either the magnitude or orientation of the magnetic field, have made the magnetothermal oscillation approach attractive as a tool for studying the electronic structure of bismuth. Since this method has revealed details in bismuth not observed by other methods,[2] there seems to be little doubt but what the method will be useful for many other materials.

When a magnetic field is applied to free electrons, the motion in a plane perpendicular to the directions of the magnetic field is quantized. This is illustrated in Fig. 1 where the magnetic field is applied along the z direction and the quantization occurs in the k_x-k_y planes of crystal momentum space. In the simple case of a spherical Fermi surface, the energy states are compressed into the walls of a series of concentric "tubes" and are highly degenerate. Within each tube of states (Landau band), the energy varies only in the k_z directions as

$$E(n,k_z)=(n+\tfrac{1}{2})(eH/m^*c)+\hbar^2k_z^2/2m^\dagger \qquad (1)$$

or

$$=(n+\tfrac{1}{2})\hbar\omega_c+\hbar^2k_z^2/2m^\dagger,$$

and is illustrated by the energy diagram on the right side of Fig. 1. $E(n,k_z)$ is the energy of an electron in the nth Landau band having momentum k_z in the z direction, where n is the quantum number of the Landau band. $m^\dagger$ is the component of the reciprocal of the inverse mass tensor. ω_c is the cyclotron frequency, e is the electronic charge, H is the magnetic field, c is the velocity of light, and m^* is the cyclotron mass. At 0°K, the bands are occupied to an energy equal to the Fermi energy, indicated by the dashed line. At temperatures other than 0°K the filling does not end abruptly at the Fermi energy but varies as the Fermi distribution function within a region of the order of k_bT of the Fermi energy, where k_b is the Boltzmann constant. In order to experimentally observe effects associated with the discrete nature of each Landau band, it is necessary that the relaxation time of the electrons, τ, be sufficiently long so that $\omega_c\tau>1$, i.e., the magnetic field be high enough and the temperature low enough that the energy separation between bands be greater than the order of k_bT, $(\hbar\omega_c>k_bT)$.

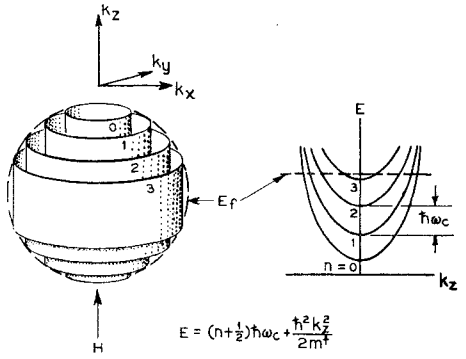

FIG. 1. Quantization of electrons in a magnetic field for the case of a spherical Fermi surface where spin is neglected. On the right-hand side the electron states are shown as compressed into a series of highly degenerate, concentric "tubes" (Landau bands). The energy of each band varies only in the k_z direction as is illustrated on the right-hand side. The "tubes" and energy bands are occupied to within k_bT of the Fermi energy which is shown by the dotted line and dotted circle.

As the magnetic field is increased from that corresponding to the situation represented in Fig. 1, the "tubes" in the left-hand figure expand. The energy of the electrons within each band increases as well as the separation between bands. In the case illustrated, the electrons from the third band are redistributed among the states of the lower energy bands as they become more degenerate. The density of states per unit energy varies as $1/k_z$ and thus reaches a maximum just as the bottom of the third Landau band passes through the Fermi surface and the band is being completely emptied. An increase in the density of states at the Fermi surface leads to an increase in the electronic specific heat and, thus, an increase in the entropy of the electronic part of the system. An increase in the entropy of the electronic subsystem increases the amount of thermal energy required to maintain the initial temperature. Since the process is adiabatic, and irreversible effects are to a first approximation neglibible, the only source of thermal energy is from the crystal lattice which, therefore, is cooled. Thus, a suitable thermal sensing element with negligible heat capacity in good thermal contact with the crystal, registers a temperature minimum (or cooling

[4] D. Shoenberg, Proc. Roy. Soc. (London) **A170**, 341 (1939).

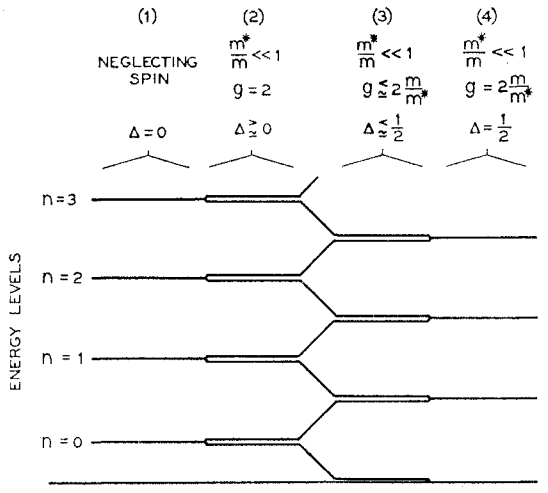

FIG. 2. Effect of various situations on the spin splitting of Landau levels for a given value of crystal momentum along the magnetic field. (1) Spin is neglected and therefore $\Delta=0$. (2) $g=2$ is used for electrons of mass much smaller than the free electron mass. (3) The g factor for electrons in bismuth is approximately equal to but less than $2m/m^*$. (4) $g=2m/m^*$ and $\Delta=\frac{1}{2}$.

peak) as the magnetic field is varied through the appropriate interval to pass the bottom of a Landau band through the Fermi surface.

The magnetothermal oscillations are a special case of adiabatic demagnetization which is usually associated with paramagnetic materials. In the case of magnetothermal oscillations, the magnetic subsystem is an electronic subsystem in which ordering processes are very much less sensitive to the magnetic field and, thus, exhibit much smaller thermal effects. There is an increase in electronic energy followed by a comparable decrease each time a Landau level passes through the Fermi surface, with the result that the process is repetitive with either increasing or decreasing magnetic fields.

There are few, if any, metals that have spherical Fermi surfaces and, in fact, most cases are quite complicated. Even so, the general behavior discussed above applies but the magnetothermal oscillations will also be orientation dependent. If the Fermi surface is ellipsoidal, as is the case in bismuth, the cyclotron mass (and thus the area of k space perpendicular to H) varies with the orientation, and each time the combination of cyclotron mass and field is appropriate, a cooling peak may result.

Consider the case of a single Fermi ellipsoid in an experiment in which the field is rotated from a direction θ, to a direction θ_2. There will be $(|n_{\theta_1}-n_{\theta_2}|-1)$ cooling peaks in the interval, where n_θ is the quantum number of the pertinent Landau level. This applied only if the interval does not include a maximum or minimum in the cross section of the Fermi surface. Using Eq. (1) and considering the conditions necessary for producing a cooling peak, it can be shown that at constant magnetic field,

$$\frac{n_{\theta_1}+\frac{1}{2}}{n_{\theta_2}+\frac{1}{2}}=\frac{m_{\theta_1}^*}{m_{\theta_2}^*}, \tag{2}$$

where $m_{\theta_1}^*$ and $m_{\theta_2}^*$ are the cylcotron masses at orientations θ_1 and θ_2, respectively. In the case of bismuth there are cooling peaks associated with each of the nonequivalent Fermi ellipsoids causing additional complications. However, each peak can and must be accounted for by a consistent representation of the Fermi surface. Conversely, such a quantity of information, as is represented by the many observed peaks, permits the determination of the detailed shape of the Fermi surface with considerable precision.

In the discussion thus far, the effect of electron spin has been neglected. Cohen and Blount[5] have shown on theoretical grounds that the spin splitting is comparable to $\hbar\omega_c$ for certain orientations of the magnetic field in bismuth, and so cannot be neglected even though m^* is small. This prediction has been confirmed in a direct microwave spin resonance experiment[6] and also in magnetothermal experiments.[2]

If the effect of spin is included, Eqs. (1) can be written in the form:

$$E=(n+\tfrac{1}{2}\pm\Delta)(\hbar eH/m^*c)+\hbar^2k_z^2/2m^\dagger. \tag{3}$$

Δ is a parameter that determines the spin splitting and is given by

$$\Delta=m^*g/4m, \tag{4}$$

where g is the spectroscopic splitting factor for the pertinent orientation and m is the free electron mass. The effect of various values of Δ on the spin splitting of the Landau levels for a given value of crystal momentum along the magnetic field is summarized in Fig. 2.

It is useful to define the Fermi energy in terms of the parameters of Eq. (3):

$$E_f=(n_f+\tfrac{1}{2}\pm\Delta)(\hbar eH_f/m^*c). \tag{5}$$

n_f is the quantum number of the Landau level at the Fermi surface and H_f is the relevant value of the magnetic field. In the consideration of the periodicity of cooling peaks with magnetic field, it is convenient to write Eq. (5) in terms of $1/H$:

$$n_f=-\tfrac{1}{2}\pm\Delta+(E_fm^*c/\hbar e)(1/H_f). \tag{6}$$

It is interesting to notice the effect that the value of Δ has on the intercept of a plot of n_f (or n_f plus an integer) against $1/H_f$ (e.g., Fig. 22). If $\Delta=0$, the intercept is $\frac{1}{2}$ (or an integer plus $\frac{1}{2}$). However, if $\Delta\simeq\frac{1}{2}$, as it is for some low mass directions in bismuth, then the intercept is nearly 0 (or integral) and accounts for the relevant observation of Dhillon and Shoenberg[7] as well as our own

[5] M. H. Cohen and E. I. Blount, Phil. Mag. **5**, 115 (1960).
[6] G. E. Smith, J. K. Galt, and R. F. Merritt, Phys. Rev. Letters **4**, 276 (1960).
[7] J. S. Dhillon and D. Shoenberg, Trans. Roy. Soc. (London) **248**, 1 (1955).

data. An analysis of experimental data by the method just described is one of the most straightforward ways of distinguishing betweeen very large and very small spin splitting.

II. EXPERIMENTAL PROCEDURE

The cryostat used for these observations is illustrated in Fig. 3. With the exception of the sample chamber which is attached to the removable head, the arrangement of the cryostat, magnet, and Hall probe is the same as was used in earlier work.[8] The sample chamber with the cryostat omitted is shown schematically in Fig. 4. The sample (a single crystal of bismuth) is supported and is thermally isolated by embedding it in silicon powder. The silicon powder was selected on the basis of its low heat capacity, freedom from magnetic impurities, and desirable thermal insulating properties. The thermal relaxation time for heat transfer between the sample and the helium bath can be varied over a wide range of values by varying the particle size of the powder.[9] (The importance of selecting an appropriate relaxation time is discussed later.) In our earliest observations aluminum oxide powder was used. Although this material was quite satisfactory for the measurements at constant field, the magnetic impurities that it contained were responsible for large adiabatic temperature changes when the field strength was varied.

The temperature sensing element is a carbon resistance thermometer that was prepared from a thin slice of a 10 Ω–2 W Allen Bradley resistor. The thermometer was placed in good thermal contact with the bismuth crystal by using either Formvar or GE No. 7031 cement and a thin (a few ten-thousandths of one inch thick) layer of Mylar for electrical insulation. Details relating to the use of this type of thermometer have been described elsewhere.[10] The thermometer was so oriented that its axis was perpendicular to the plane of rotation of the magnetic field. In this orientation any variation of resistance of the thermometer with rotation of the magnetic field was negligible. Temperature changes are observed by keeping the thermometer current constant and biasing out the majority of the potential drop with a potentiometer. The unbalanced voltage is amplified and recorded on a recorder. Except for a magnetoresistance contribution, when the magnitude of the magnetic field is varied, the recorded voltage changes are proportional to the temperature changes of the sample.

Because the power dissipated by the thermometer must be transferred to the helium bath, the use of an appropriate fine powder for support makes it possible to thermally isolate the sample to a degree far beyond that which can be profitably utilized. It is apparent that one wants to select a thermometer that will have the maximum temperature detection sensitivity. Although excellent results were obtained in the present study without the necessity of exploiting this point, the success of future magnetothermal observations in other metals may depend on the extent to which the temperature sensitivity of the thermometer is enhanced. Assuming that a more sensitive device than a resistance thermometer is not developed, there are two ways in which the sensitivity can be increased: (1) By selecting the material for the thermometer and its resistance to give the optimum performance. The sensitivity, $R^{-1}\,dR/dt$ of a thermometer, varies with the composition and the resistivity of materials. For many semiconductors $R^{-1}\,dR/dt$ increases with increasing resistivity. For example, in the case of arsenic-doped germanium[11] $R^{-1}\,dR/dt \propto R^{\frac{1}{2}}$ (for a specified configuration). To the extent that the available instrumentation permits completely effective operation, there is a gain in sensitivity in this case by going to thermometers constructed of higher resistivity material, at the rate of $R^{\frac{1}{2}}$. However, insulation resist-

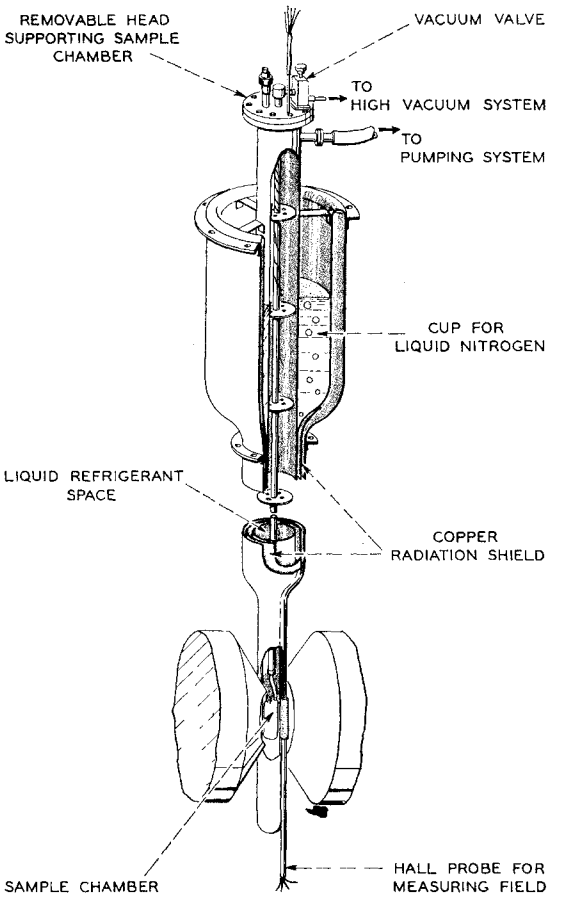

FIG. 3. Arrangement of cryostat, magnet, and Hall probe. The sample chamber and electrical leads are attached to the removable head.

[8] C. Herring, T. H. Geballe, and J. E. Kunzler, Phys. Rev. **111**, 36 (1958).
[9] J. E. Kunzler (to be published).
[10] W. S. Boyle and K. F. Rodgers, J. Opt. Soc. Am. **49**, 66 (1959).
[11] J. E. Kunzler, T. H. Geballe, and G. W. Hull, in *Temperature —Its Measurement and Control in Science and Industry* [Reinhold Publishing Company (to be published)].

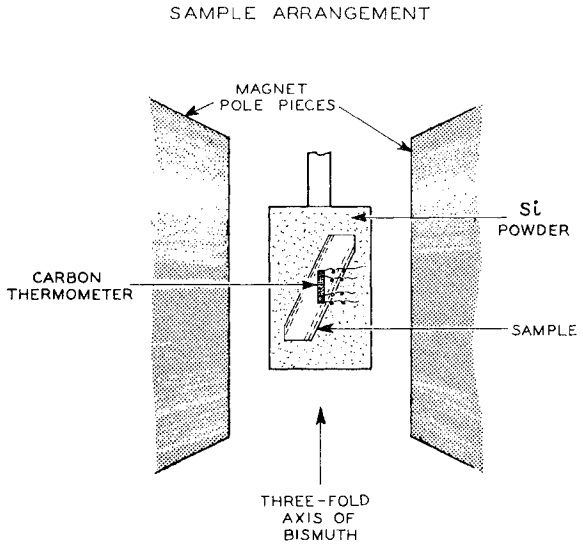

FIG. 4. Sample arrangement. The sample, a single crystal of bismuth embedded in silicon powder within the sample chamber, is shown between the pole pieces of the magnet. The cryostat is omitted.

ance and instrumentation capabilities result in a limited advantage in this direction. (2) By making an optimum choice of thermometer current and thermal relaxation time (between the sample and the helium bath), the temperature sensitivity can be improved. The selection will depend on the information desired from the experiment. For a short thermal relaxation time, more current can be used and thus a higher temperature sensitivity will be achieved. However, the peaks are then distorted. Such distortion is generally not serious if only the existence and location of peaks are desired, rather than quantitative data with respect to their magnitude. Clearly a judicious compromise, which is dependent on the nature of the information required, must be made for each type of observation. There are, of course, other factors which must be considered such as the rate at which the field is swept or the rate at which the magnetic field is rotated.

In the current work, a thermal relaxation time between the sample and the helium bath of several minutes and a sweep rate of the magnetic field of approximately 1 kG per min were generally used. For the rotational data, the rate of rotation was usually about 20 deg per min. In a typical observation it was found that 4×10^{-7} W of energy dissipation by the thermometer resulted in a difference in temperature between the sample and the helium bath of 0.05°K when the thermal relaxation time was about two minutes. This arrangement permitted the detection of temperature changes of 10^{-5}°K.

The magnetic field strength was measured by using a Hall probe[12] that was calibrated against nuclear resonance probes. It is accurate to 0.1% and reproducible to 0.01% over the range of fields used.

[12] T. H. Geballe and J. E. Kunzler (to be published).

The sample of bismuth is from a single crystal grown by Wernick[13] from zone-refined bismuth. The crystal was produced by spontaneous nucleation during the last pass of the zone-refining operation. The portion of the crystal selected was cut from the lead end of the crystal using an acid string saw. The resistance ratio,

$$R_{273°K}/R_{4.2°K},$$

along the trigonal axis was measured using the entire sample and found to be 210. The sample is about 3cm×1cm×0.6cm with the threefold axis approximately 20 deg from the longest dimension. It weighs approximately 15 g. The sample was oriented such that the plane of rotation of the magnetic field was perpendicular to the threefold axis of the bismuth crystal and thus the twofold (binary and bisectrix axes) were in the plane of rotation.

In the rotational experiments, a field is selected, and the magnet is rotated at a uniform rate of about 20 deg per min. It was found that varying the rate of rotation by a factor of 4 changed the magnitude of the peaks by nearly 10% as one would expect from the magnitude of the thermal relaxation time between the sample and bath. However, the pertinent features are not altered. Reversing the direction of rotation of a magnetic field shifts the position of the peaks by less than a few tenths of a degree, demonstrating that the thermal relaxation time between the thermometer and the sample is short.

The positions of the peaks as a function of the magnetic field are obtained from rotational data by first

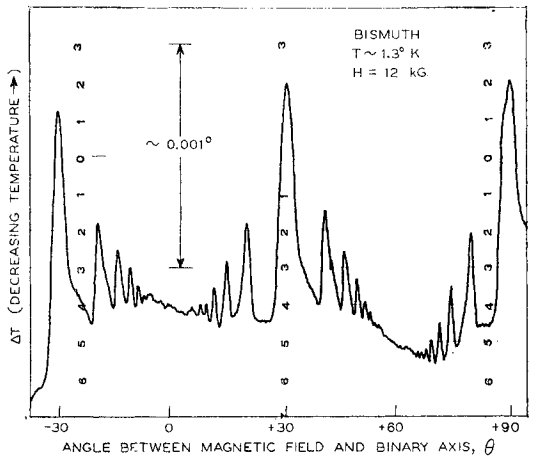

FIG. 5. Recorder tracing of rotational cooling peak pattern at 12.00 kG. The plane of rotation of the magnetic field is perpendicular to the threefold axis. The principal peaks ($p_a=1$, $p_b=2$) are bisectrix peaks (−30°, +30°, and 90°) and are in the direction of cooling. There are no binary peaks (0° and +60°) at 12 kG. The principal peaks are about 0.001°K in magnitude which represents 2 ergs of energy for this sample. The existence of a series of peaks that decrease in magnitude with distance from the bisectrix peaks is quantitatively consistent with the over-all data. The total instrumental noise can be determined from data at $\theta=0°$ and $\theta=+60°$.

[13] J. H. Wernick, K. E. Benson, and D. Dorsi, Trans. AIME 209, 996 (1957).

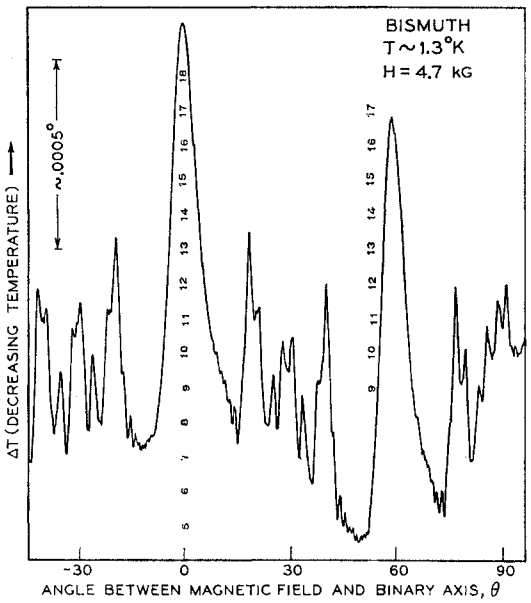

FIG. 6. Recorder tracing of rotational cooling peak pattern at 4.70 kG. The plane of rotation of the magnetic field is perpendicular to the threefold axis. The principal peaks ($p_a=3$) are binary peaks at 0° and +60°. The bisectrix peaks (no contribution from group a, $p_b=5$) at −30°, +30°, and +90° are reduced and split. The effect of a misalignment of the order of a degree is apparent from the splitting of the bisectrix peaks.

making observations at a series of fixed field intervals in order to establish the characteristic features. Once the value of the magnetic field corresponding to the pertinent peak is approximately known, a series of rotational observations are made at fields near that of the peak under study.

Observations at constant angle were made by sweeping the field at a uniform rate of about one kG per min. Decreasing the rate of sweep by a factor of 2 or 3 from this value reduced the height of the peaks by several percent, but there was no detectable shift in the location of the peaks.

III. EXPERIMENTAL RESULTS

Oscillations vs Orientation at Constant Field

Copies of recorder tracings that show typical cooling peak patterns that were observed at 1.3°K as the orientation of the magnetic field was varied while at constant field strength, are shown in Figs. 5, 6, and 7. These observations were taken at 12, 4.7, and 1.1 kG, respectively, and illustrate typical behavior at high, medium, and low fields in bismuth.

The cooling-peak pattern shown in Fig. 5 is one of the earliest ones, taken at a time when the magnet was rotated by hand. In this and similar figures, decrease in temperature with respect to some arbitrary reference is recorded against the orientation of the magnetic field. The angle θ is measured between the magnetic field and a particular binary axis. The trigonal axis of the crystal coincides with the axis of rotation so the patterns repeat every 60 deg. Midway between the binary axes (i.e., $\theta=\pm30°$, etc.) there are three bisectrix axes, which like the binary axes have twofold symmetry. The most pronounced peaks occur either with the field along one of the binary axes or one of the bisectrix axes as would be expected from the consideration of the symmetry and the band structure of bismuth (discussed later). In Fig. 5 the principal peaks are along the bisectrix axes, and there is a series of smaller peaks on either side, five of which are clearly distinguishable and have been accounted for. It should be noted that the pronounced peaks are cooling peaks and also that there are no peaks with the field parallel to the binary axis at a field of 12 kG.

The bisectrix peaks (H parallel to a bisectrix axis) in Fig. 5 are near their maximum magnitude which occurs at 12.3 kG (see fourth column of Table I). The magnitude of these peaks is about 0.001°K which in terms of energy represents about 2 ergs for our particular sample. The maximum cooling peak that we have observed in bismuth is a binary peak of 0.003°K. The total instrumental noise in Fig. 5 is a few hundred thousandths of a degree and can be seen at $\theta=0°$ and $\theta=+60°$.

The lack of perfect symmetry about the principal peaks can arise from a number of sources: (1) variations in the helium-bath temperature, (2) eddy-current heat generation, (3) mechanical vibrations, and (4) a decrease in the heat transferred between the sample and the helium bath when the sample temperature decreases as a peak is produced. This latter behavior also has the effect of reducing the height of the peaks a few percent depending on the rate of magnet rotation as was mentioned earlier. The satellite peaks (i.e., smaller peaks occurring with the magnetic field along nonsymmetry

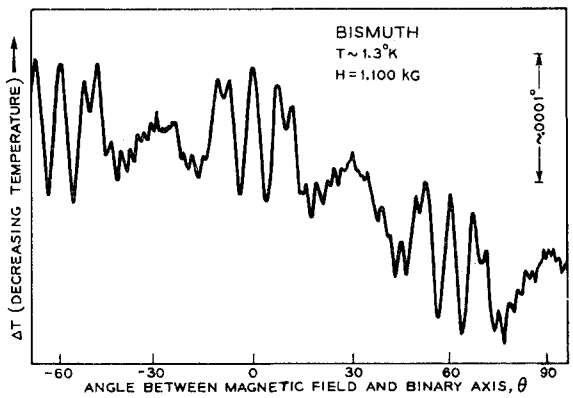

FIG. 7. Copy of recorder tracing of rotational cooling peak pattern at 1.100 kG. The plane of rotation of the magnetic field is perpendicular to the threefold axis. The most prominent peaks are binary peaks ($p_a=13$) at −60°, 0°, and +60°. The next peaks on either side of the binary peaks ($p_a=14$) are due to the next higher Landau level. The bisectrix peaks ($p_a=11$, $p_b=22$) at −30°, +30°, and +90° are part of an envelope of closely spaced peaks from higher numbered Landau levels. The total instrumental noise is about 10^{-5}°K which is of the same magnitude as these latter peaks.

TABLE I. Field dependence of cooling peaks observed in bismuth with the plane of rotation of the magnetic field perpendicular to the threefold axis. The peak number, p (column 1), is p_a for the binary peaks of column 2 and p_b for the bisectrix peaks of column 4. The lower mass series of bisectrix peaks (p_a) are also included in column 4 since they are superimposed on alternate higher mass peaks and are designated by the footnotes. Their peak numbers, p_a, are one-half of those given in column 1 and their value of $10^7/p_bH$ is thus twice that of column 5. The much higher mass series of binary peaks, p_b, were not sufficiently well resolved to warrant inclusion in the table. The observed spin splitting is indicated by the two values in the table for the two binary peaks with $p_a=1$.

p	$H\|\|$binary axis		$H\|\|$bisectrix axis	
	H in gauss	$10^7/p_aH$	H in gauss	$10^7/p_bH$
1	{15 500 14 200±100}	673	...	...
			...	...
2	7150±50	700	[a] 12 300±200	406
3	4720±30	703	8150±50	409
4	3750±20	700	[a] 6130±50	408
5	...	...	4900±30	408
6	...	...	[a] 4100±40	406
7	...	...	3500±30	408
8	1785±5	700	...	...
13	1098±5	701	...	...
14	...	...	[a] 1740±10	410
22	...	...	[a] 1113±5	408

[a] Represents two superimposed peaks ("double" peaks).

directions) are not necessarily expected to have the same slope on either side of the peak and, in fact, do not—as can be seen from the figures.

It is convenient to describe each observed cooling peak of a series in terms of an experimental parameter which will be referred to as the peak number, p. The numerical value of p for the peaks is determined by plotting $1/H$ vs p (or p plus an integer) and by assigning the number 1 to the first peak at $1/H>0$, 2 to the peak with next higher value and so on. In the case where some of the peaks in a series are slightly separated due to electron spin, the same peak number, p, is assigned to each of the split peaks, that is, each pair is considered as one unit in the assignment of numbers (this treatment is appropriate for all cases involving spin splitting in this report). However, if the spin splitting is such that all observed peaks are resolved, then they can be treated as separate series. In general, for a given direction of the magnetic field there may be more than one nonequivalent group of electrons and/or holes each producing a series of peaks. Different series of cooling peaks produced by different groups of carriers are distinguished by using the subscript a, b, c, etc., where p_a refers to the lowest mass series of peaks since they are the most likely to be observed. For arbitrary directions of the magnetic field in the plane perpendicular to the threefold axis of bismuth, the data can be described in terms of three nonequivalent groups of electrons and one nonequivalent group of holes (not observed in the data being reported). Along symmetry directions (e.g., binary and bisectrix axes) the number of nonequivalent groups of electrons reduces to two for each direction.

It happens that each bisectrix peak of Fig. 5 is the result of a contribution from two groups of electrons (one having almost exactly one half the cyclotron mass of the other) and, thus, each peak has two peak numbers (e.g., $p_a=1$ and $p_b=2$).

The cooling peak pattern at 4.7 kG shown in Fig. 6 was made using a mechanical drive on the magnet. In this case each principal peak is a binary peak ($p_a=3$) and has about the same magnitude as the bisectrix peaks at the higher field shown in Fig. 5. Bisectrix peaks are also present in Fig. 6. However, at this field they are considerably reduced from their maximum value and are split—a behavior that is often observed and will be explained later.

One feature of decreasing the magnetic field is to increase the number of peaks that are produced in a given angular interval. This is due to the fact that the energy levels are more closely spaced and, thus, more pass through the Fermi surface during the rotation of the magnetic field through the interval than at the higher field. The noticeable difference in the detailed shapes of the peaks in different, but equivalent, sections of the pattern (e.g., splitting of bisectrix peaks at −30 deg, +30 deg, and +90 deg) is attributed to a slight mis-

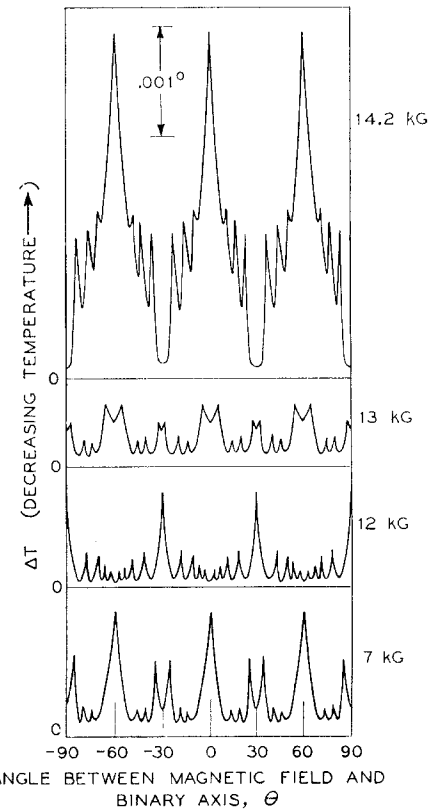

FIG. 8. Composite of rotational cooling peak patterns based on experimental data that illustrates how patterns vary with magnetic field. The field dependence of binary peaks (+60°, 0°, −60°) and bisectrix peaks (+90°, +30°, −30°, −90°) can be seen. The field dependence shown by these rotational patterns is consistent with observations involving field variation at constant orientation as is expected.

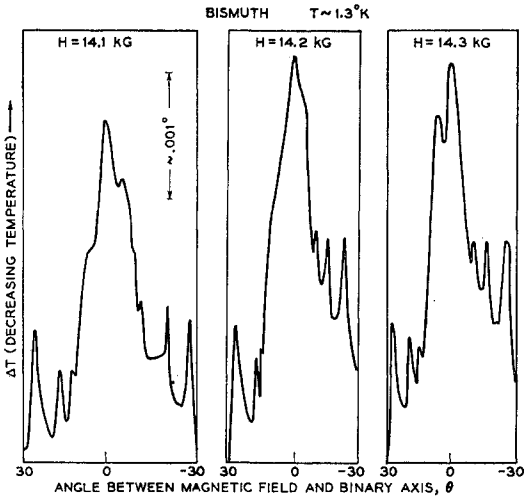

FIG. 9. The splitting of a binary cooling peak ($p_a=1$) observed at three closely spaced fields. The variation of the peak splitting with field is used to locate the field corresponding to the peak maximum (14.2±0.1 kG).

orientation of the sample, probably of the order of a degree. Examination of the data shows that this effect has not led to significant inaccuracies in locating the positions of the peaks with respect to the magnetic-field intensity.

The cooling-peak pattern from a rotational diagram at 1.1 kG shown in Fig. 7 is for the lowest field at which measurements were made. The principal peaks are the 13th binary peaks ($p_a=13$). The peaks immediately on either side of each binary peak ($p_a=14$) originate from the next higher Landau level and are almost as high as the binary peaks, as expected. The bisectrix peaks are so closely spaced that only the tops are apparent in the form of an envelope. Even so, it was possible to locate the field at which the bisectrix peaks become a maximum with an accuracy of about 1%. The peak numbers of the bisectrix peaks (each is a "double" peak) are $p_a=11$ and $p_b=22$.

The magnitude of the binary peaks in Fig. 7 is about 10^{-4}°K. The total instrumental noise is about 10^{-5} deg. As mentioned earlier, the sensitivity can be increased and it has been since these data were taken.

Figure 8 is a composite sketch based on observed cooling-peak patterns which illustrate how the rotational patterns vary with magnetic field. One of the strongest peaks observed is a binary peak ($p_a=1$) at 14.2 kG. At this field there are no bisectrix peaks. As the field is lowered to 12 kG, the binary peak is completely absent as can also be seen from Fig. 5. As the field is further decreased another binary peak ($p_a=2$) again becomes prominent and reaches a maximum near 7 kG. This behavior repeats until the 13th peak ($p_a=13$) is observed near 1.1 kG (Fig. 7). In addition to this series of peaks, there is a series of higher-mass binary peaks ($p_b=1, 2, 3,$ etc.), which are only a few hundred thousandths of a degree in magnitude, that have been detected only above 16 kG where they are not masked by the much more prominent lower mass peaks. Since the spacing of the higher-mass peaks is of the order of 1 kG it will be necessary to extend our measurements to fields above the maximum used in this work (18 kG) in order to study their behavior.

Referring again to Fig. 8, as the magnetic field is decreased from 14.2 kG where there are no bisectrix peaks, a "double" bisectrix peak ($p_a=1$, $p_b=2$) begins developing just above 13 kG and is fully developed at 12.3 kG. It has become somewhat reduced at 12 kG. As the field is further reduced, the peak disappears and a new and "single" peak ($p_b=3$) is fully developed at 8.15 kG. By the time the field is lowered to 7 kG, it is split into a doublet which disappears as the field is decreased further. The process repeats as the field is further decreased until the 22nd peak in the p_a series and the 11th in the p_b series appear as a "double" peak at about 1.1 kG.

The positions of the various peaks in the patterns and their variation with magnetic field are consistent with observations in which the magnitude of the field was varied while the orientation was kept constant. This consistency is, of course, to be expected.

The location of a peak, with respect to magnetic field and the separation of the peaks in terms of $1/H$, can be determined conveniently and most accurately from rotational measurements at constant field as was mentioned earlier. It has been possible to locate the positions of the binary and bisectrix peaks to better than 1% using the following method: Once the approximate field at which a peak occurs is known, several rotational diagrams were taken at sufficiently closely spaced field intervals to pinpoint the field that is required to produce the peak at its maximum height. At the higher fields it is often possible to make use of the splitting of the peaks as an aid in locating the maximum (not all peaks show splitting as is discussed in the section on comparison of experiment with theory) as is illustrated

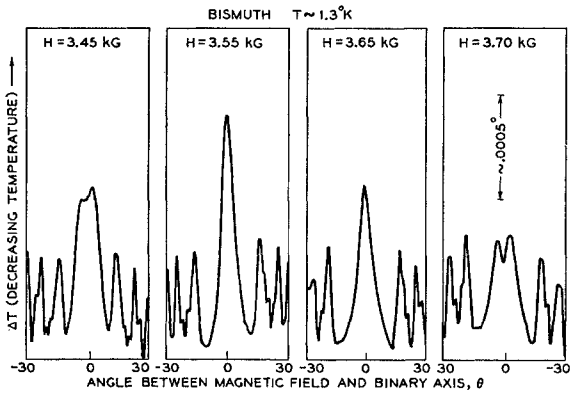

FIG. 10. Variation of the cooling peak patterns of a binary peak ($p_a=4$) with magnetic field at closely spaced field intervals near that at which the peak is a maximum. Using these four patterns and others not shown a value of 3.57±0.02 kG is obtained for the field representing the peak maximum.

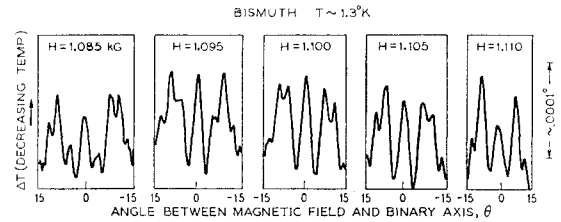

FIG. 11. Variation of the cooling peak patterns of the 13th binary peak ($p_a=13$) with magnetic field at closely spaced intervals near that at which the peak is a maximum. By making use of the neighboring peaks ($p_a=14$, 15, etc.), a value of 1.098±0.005 kG is obtained for the field representing the peak maximum.

in Fig. 9 for binary peaks near 14 kG. The cooling peak pattern near a binary peak is shown for fields of 14.1, 14.2, and 14.3 kG. From the height and the splitting of the peaks at fields above and below 14.2 kG, it is apparent that the maximum is near 14.2 kG.

At lower fields the splitting of the peaks is not helpful since the field difference between splitting on the high-field and the low-field sides of the peak does not decrease appreciably with decreasing field as does the spacing between peaks. Figure 10 shows the behavior of the fourth binary peak ($p_a=4$) at a series of fields near 3.5 kG. Using the heights of the peaks from these patterns, and several not included, a value of 3.57±0.02 kG was assigned for the magnetic field of the peak.

Peak patterns near 1.1 kG are shown for the 13th binary peak ($p_a=13$) in Fig. 11. At these low fields the satellite peaks on either side are helpful in pinpointing the maximum of the principal peak. A value of 1.098±0.005 kG was determined for this peak.

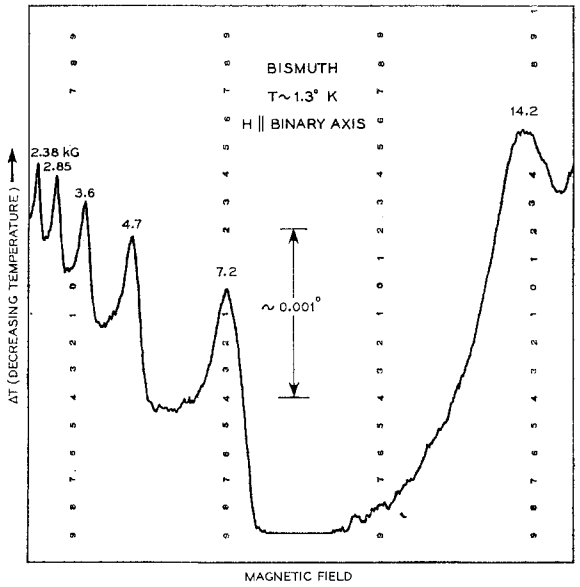

FIG. 12. Recorder tracing showing cooling peaks as a function of magnetic field for the field along the binary axis as the magnetic field was increased. The value of magnetic field noted for each peak is obtained from rotational data which permit more precise assignments.

The fields at which binary peaks have been observed are summarized in the second column of Table I. The peak number is given in the first column. Since the intercept of a plot of p_a vs $1/H$ is very near 0, the values of $10^7/p_aH$ tabulated in the third column are, among other things, an indication of the accuracy of the data. Observations were not made to pinpoint the location of other peaks merely because there seemed to be relatively little to be learned by so doing. The pair of binary peaks that correspond to $p_a=1$ and occur at 14.2 and 15.5 kG are separated (and are the only pair in the table separated) by spin splitting. The average value of 14.85 kG was used for computing their value in column 3. The deviation of this value from the others is not believed to be a consequence of spin splitting but is thought to be the result of an entirely different type of phenomenon. This phenomenon and spin splitting are discussed in the appropriate sections.

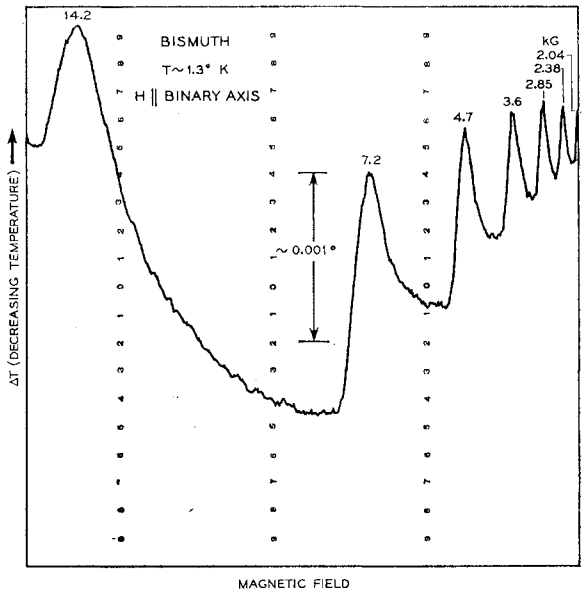

FIG. 13. Recorder tracing showing cooling peaks as a function of magnetic field along the binary axis as the magnetic field was reduced. Since the experimental factors that govern the behavior of the "apparent base temperature" were as identical as practical with those for Fig. 10 (except that the magnetic field was being increased for Fig. 10) and the curves are very similar, it follows that the main features of the curves are reversible properties of the bismuth (and the thermometer) rather than a result of irreversible experimental temperature changes. It can thus be shown that the asymmetry of individual peaks is a characteristic property of bismuth and does not arise from experimental procedures. The values of the magnetic field noted for each peak are from rotational data which permit more precise assignments.

The data for the bisectrix peaks are summarized in column 4 of Table I and were determined in much the same manner as described above for binary peaks. However, it was observed that alternate peaks were higher than would be expected from the sequence, and also a bit broader with respect to field variation. This led to a somewhat larger uncertainty in pinpointing the mag-

netic field, as can be seen from the uncertainties assigned to values in the table. These higher peaks ("double" peaks) are the result of a second series of bisectrix peaks having a mass almost exactly one-half that of the first series as was discussed earlier. (Also see Fig. 14.)

Oscillations vs Magnetic Field Strength at Fixed Orientation

Observations of the cooling peaks as a function of the magnetic field at constant orientation of the magnetic field are shown in Figs. 12, 13, and 14. In these figures, the variation of the "apparent base temperature" is chiefly due to the combined effects of the magnetoresistance of the thermometer and the temperature coefficient of the nonoscillatory part of the susceptibility. Eddy-current heating and changes in the bath temperature may have also contributed. The magnetoresistance

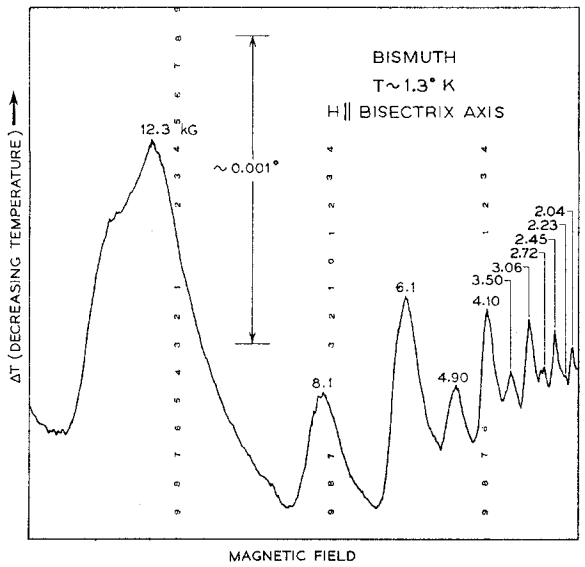

FIG. 14. Recorder tracing showing cooling peaks as a function of the magnetic field for the field along the bisectrix axis as the field was increased. The value of the magnetic field noted for each peak is from rotational data which permit more precise assignments. The enhancement of alternate peaks of one series ($p_b=2$ to $p_b=12$ at 12.3, 8.1, 6.1 kG, etc.), by peaks from a lower mass series ($p_a=1$ to $p_a=6$ at 12.3, 6.1, 4.10 kG, etc.) having a cyclotron mass almost exactly one-half that of the first series, is clearly evident. The distortion of the top of the 12.3-kG peak ($p_a=1$ and $p_b=2$) is evidence that the spin splitting parameter, Δ, is not exactly one-half for one or both groups of electrons.

was negligible at low fields but increases as H^2, and amounted to about one percent of the resistance of the thermometer at 18 kG. In terms of temperature this is equivalent to several thousandths of a degree at 18 kG. Incidentally, the behavior of the base temperature with the field parallel to the binary axis would not be expected to be necessarily the same as with the field parallel to the bisectrix axis, since susceptibilties are in general different. (Similarly the eddy-current heating contribution will be different since the electrical conductivity is

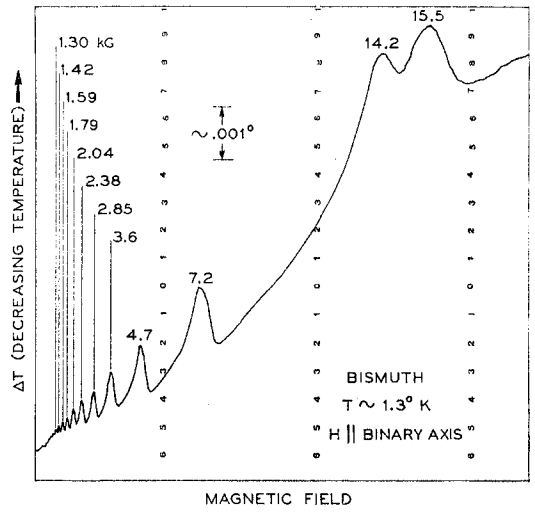

FIG. 15. Recorder tracing showing cooling peaks as a function of the magnetic field for the field along the binary axis as the field was decreased. The value of the magnetic field noted for each peak is from rotational data which permit more precise assignments. The spin splitting is evident for the $p_a=1$ peaks (14.2 kG and 15.5 kG) but not for the peaks at lower fields.

also anisotropic.) The contribution to the "apparent base temperature" from the magnetoresistance of the thermometer is the same for both orientations since the magnetoresistance of the thermometer is not orientation dependent.

From an examination of Figs. 12 and 13, it is apparent that the individual peaks are not symmetrical and that this is not a consequence of eddy-current heating or of a change in the thermal relaxation time to the helium

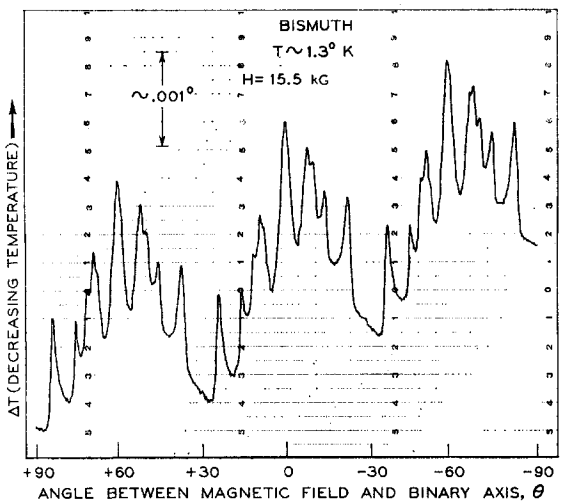

FIG. 16. Recorder tracing at 15.5 kG showing the spin splitting of the $p_a=1$ peak near the binary axis. The plane of rotation of the magnetic field is perpendicular to the threefold axis. The $\theta=0$ peak is the same one observed at 15.5 kG in Fig. 13. The $\theta=\pm 8°$ peaks would appear as a single peak if the effect of spin splitting was unresolved. The remaining peaks (in each 60° interval) are from the higher mass electrons (p_b series of peaks) and have been accounted for quantitatively.

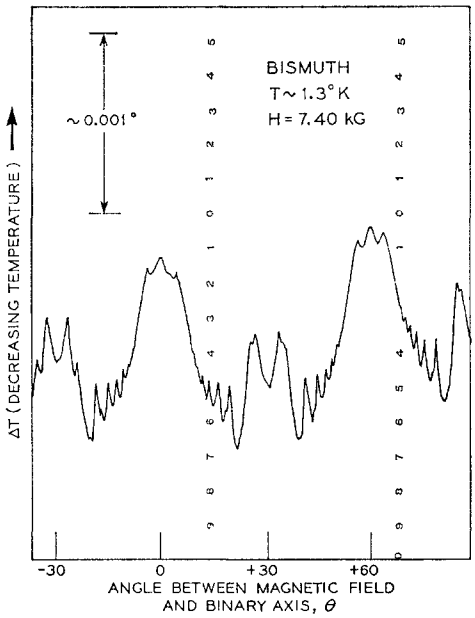

FIG. 17. Recorder tracing at 7.40 kG showing the spin splitting of $p_a=2$ peak near the binary axis. The plane of rotation of the magnetic field is perpendicular to the threefold axis. The peaks at $\theta=-4°$, 0°, and +4° (also +56°, 60°, and 64°) are related to the spin splitting in the same way as the peaks of Fig. 14. It is not possible to account for the three central peaks as originating from other currently known sources. The five satellite peaks on each shoulder originate from the higher mass group of electrons (p_b series of peaks).

bath. The change in temperature with magnetic field is clearly much slower on the low-field side of each peak than on the high-field side. If the temperature were recorded against $1/H$ instead of H, the lack of symmetry would become even more apparent. This behavior is consistent with elementary considerations of the quantitative features of the phenomena which give rise to cooling peaks and will not be discussed further in this report.

In Fig. 14, the enhancement of alternate members of a series of bisectrix peaks ($p_b=2$ to $p_b=12$) by the series of lower mass peaks ($p_a=1$ to $p_a=6$) to give "double" peaks is clearly shown. The cyclotron mass of the p_a series is almost exactly one-half that of the p_b series.

Observations Pertaining to Spin Splitting

When the spin-splitting parameter, Δ, is 0 or $\frac{1}{2}$, the effect of spin is not generally apparent in the experimental observations. However, the effect of spin in bismuth is significant as has been briefly reported by us earlier.[2] The experimental manifestation of the spin splitting with the magnetic field along the binary axis is shown in Figs. 15, 16, and 17.

In Fig. 15 is shown a recorder tracing of ΔT vs H similar to Figs. 12 and 13 except that it extends to higher fields. The doublet consisting of peaks (both are $p_a=1$ peaks) at 14.2 and 15.5 kG is due to the spin splitting of the Landau levels. If turns out that the spin splitting is sufficiently large that Δ is nearly $\frac{1}{2}$ and the peaks from different Landau sublevels almost coincide and are thus difficult to observe experimentally. The splitting of the peaks at lower fields is not resolved since the separation of the peaks is small and varies as H^2. The quite different behavior of the "apparent base temperature" from that of Figs. 12 and 13 is due to the contribution of an appreciable irreversible temperature change as a result of a change in experimental variables. The distortion of the 12.3 kG peak of Fig. 14 is evidence for the existence of spin splitting in the bisectrix direction by at least one of the two contributing groups of electrons.

The resolution of the spin splitting of peaks is better with rotational observations. Fig. 16 is a recorder tracing observed at 15.5 kG. The peak at $\theta=0$ is the same peak observed at 15.5 kG in Fig. 15. The 14.2 kG peak of Fig. 15 shows up as the peaks at $\theta=+8°$ and $\theta=-8°$ in Fig. 16. The other three peaks on either shoulder, that get progressively larger as $|\theta|$ gets larger, are associated with a group of electrons of higher mass (p_b series of peaks) and have been accounted for quantitatively. If the spin splitting were not resolved, the three central peaks of Fig. 16 ($\theta=0°$, $\theta=\pm 8°$) would appear as a single peak as would the 14.2-kG and 15.5-kG peaks of Fig. 15. The peak number of each of the three central peaks of Fig. 16 is $p_a=1$.

Although the 7.2-kG binary peak ($p_a=2$) is not well enough resolved to show the effect of spin splitting in Figs. 12, 13, and 15, the splitting is resolved in the rotational observations at 7.40 kG shown in Fig. 17. The three peaks at −4°, 0°, and +4° (also at 56°, 60°, and 64°) illustrate the spin splitting in a manner similar to that described in Fig. 16. Although these peaks are not as much larger than the recorder noise as might be desired, they have been consistently observed in repeated observations. Quantitative considerations in terms of the peaks expected in this region rule out their origin as being from any other known source. The five satellite peaks on each shoulder are due to the higher mass group of electrons (p_b series of peaks) and decrease in magnitude as the binary direction is approached; the last one that is readily defined occurs at $\theta\simeq\pm 10°$.

IV. CONSIDERATION OF RESULTS

Although our investigation of bismuth is not complete, the data can be fitted to theory in a satisfying manner. First, the qualitative form of the curves of ΔT vs the magnitude or the direction of the magnetic field can be explained in terms of existing models for the Fermi surface of bismuth. It is informative to consider the structure of these curves since the approach used is relevant to other materials. Second, a value for the spin-splitting parameter, Δ, is obtained that is consistent with theoretical predictions and third, values for the cyclotron masses and the Fermi energy can be derived that are in internal agreement and in good agree-

ment with values obtained by other observers using different methods.

Structure of Observed Curves

The ΔT vs H curves, such as Figs. 12, 13, and 14, have the general shape of the susceptibility vs H curves of de Haas and van Alphen[14] and Shoenberg[4] (i.e., the peaks are periodic in $1/H$ and increase in magnitude with increasing fields). However, since the magnetothermal curves are related to the temperature coefficient of the susceptibiltiy they differ in detail. The magnitude of the peaks varies roughly as $1/p$ except in the case of superimposed peaks in which case the components of the peak from each series appear to vary as $1/p$ of the relevant series.

The rotational cooling peak patterns (e.g., Figs. 5–7, 16, and 17) are complex and contain a wealth of information useful for determining the number and shapes of the relevant Fermi surfaces. The following pieces of information are used to correlate cooling-peak patterns with the shape of the Fermi surface:

(1) Each time a cooling peak is produced a Landau level passes through the Fermi surface.

(2) The magnitude of the cooling peaks decreases with increasing peak number.

(3) The magnitude of a cooling peak of a given peak number (or quantum number) decreases with increasing mass.

(4) The spacing of peaks in $1/H$ is inversely proportional to the extreme area of k space in a plane perpendicular to the direction of the magnetic field[15] as well as to the cyclotron mass of the carriers in the appropriate Landau level.

(5) The cyclotron mass of peaks arising from carriers associated with the same Fermi surface can be related to each other by means of Eq. (2).

For a substance with a single closed Fermi surface, the determination of the shape of the Fermi surface would appear to be a reasonably straightforward process. However, since the goal of this report is not primarily concerned with the details for bismuth but rather with the broader features of magnetothermal oscillation, a simple method will be used to explain the shapes of the rotational diagrams. The approach taken is to start by explaining how a rotational diagram will appear for a single Fermi ellipsoid and "build up" to the expected behavior for bismuth.

Consider the case of the simple Fermi ellipsoid illustrated on the left side of Fig. 18 where the plane of rotation of the magnetic field is that of the maximum cross section of the ellipsoid. θ is the angle between the magnetic field and the direction where the cyclotron mass is

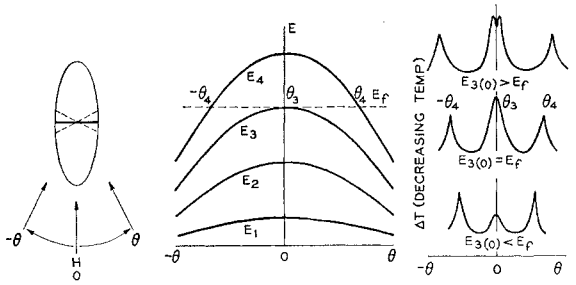

FIG. 18. The effect of the angular dependence of Landau levels on the cooling peak pattern of a simple Fermi ellipsoid. The plane of rotation of the magnetic field is parallel to the maximum cross section of the ellipsoid shown on the left side. The variation of the energy of several Landau levels with angle of the magnetic field is shown for the region near the minimum cyclotron mass in the center of the figure. Cooling peak patterns for situations are shown on the right side: (1) At the top, the magnetic field is such that the maximum value of E_3 is greater than E_f by an amount somewhat greater than k_bT. (2) In the middle, the field has been lowered to where $E_3=E_f$, and (3) at the bottom, the field is further lowered to where E_3 is less than E_f by an amount of nearly k_bT.

the minimum (i.e., the cross-sectional area of the Fermi ellipsoid is a minimum as indicated by the heavy line). The spacing between Landau levels is thus a maximum for $\theta=0$ and vary nearly as $1/m^*$ or $1/A$, such as illustrated in the center diagram of Fig. 18. The rotational diagram expected for this simple situation is shown in the center of the right side of Fig. 18. The cooling-peak pattern for increased magnetic field (increased energy for each of the levels) is shown at the top and for decreased field at the bottom. The rotational diagram in the center of the figure has three peaks since three Landau levels are passing through the Fermi surface in the angular interval shown. These are indicated by $-\theta_4$, θ_3, and θ_4. The peak due to the third level passing through the Fermi surface at $\theta=0$ indicated by θ_3 is the highest since it is due to the lowest value of n (i.e., electrons are divided between three levels for $\theta=\theta_3$ and four levels for $\theta=\pm\theta_4$). However, the side peaks are less than $\frac{3}{4}$ of the center peak since the cyclotron mass is also larger. The center peak is the broadest since the third level is within a distance k_bT of the Fermi energy over a greater angular distance than are the side peaks.

As the magnetic field is increased the third level moves above the Fermi energy and the level will broaden. Finally, when the level has moved up by an amount of the order of k_bT it will cross the Fermi surface at two distinct places and the cooling peak will split into a doublet as shown at the top of the right side of Fig. 18. It should be noted that the height of the split peak will be slightly less than the unsplit peak since each of the split peaks then corresponds to a slightly greater mass but to the same Landau level. The effect on the two side peaks at θ_4 and $-\theta_4$ of increasing the field is to separate them further and thus reduce their height slightly. As the field is further increased the center peak forms two separate peaks which continue to move apart. Finally, if the field is increased to where the second level comes within the order of k_bT of the Fermi surface a new peak

[14] W. J. de Haas and P. M. van Alphen, Communs. Phys. Lab. Univ. Leiden **212a**, (1930); **220d**, (1932).

[15] D. Shoenberg, in *Progress in Low-Temperature Physics* (North-Holland Publishing Company, Amsterdam, 1957), Vol. II, p. 226.

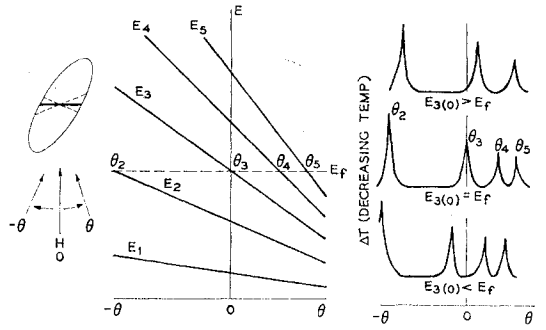

FIG. 19. The effect of the angular dependence of Landau levels on the cooling peak patterns of a simple Fermi ellipsoid similar to that of Fig. 18 except that the direction of the magnetic field corresponds to an intermediate cyclotron mass. The mass increases continuously as the magnetic field is rotated from $-\theta$ to $+\theta$. The Landau levels and the cooling peaks are more closely spaced than in Fig. 19, with the spacing being the closest in the direction of $+\theta$. As the magnetic field is increased, the cooling peaks shift to the right. Also, each peak decreases in magnitude due to its shift to a higher mass direction.

will start developing at $\theta=0$ and will become a maximum when $E_2=E_f$ (the rotational diagram for the situation where E_3 is nearly k_bT less than E_f is shown on the lower right of Fig. 18).

If the Fermi ellipsoid of Fig. 18 is rotated 90° in the plane of the magnetic field, the field will be in the highest mass direction when $\theta=0$. The energy-level diagram will then have many more levels and their spacing will be a minimum at $\theta=0$. Thus, the E vs θ curve will be concave upward. Each of the three rotational diagrams will have many more and much smaller cooling peaks than does the low mass direction case. The peak at $\theta=0$, although still the broadest, will now be smallest. The splitting of cooling peaks will then occur when the field is reduced rather than increased and the peak at the center will fade away as the field is increased. For the orientation of the maximum mass, increasing the field will cause a pair of equivalent peaks to move together. Continued increase of the field causes them to collect into a split peak and finally coalesce into a single peak when $E_n=E_f$. Further increase of the field will cause the peak to fade away.

If one were to make a series of rotational diagrams, each at a slightly higher field than the preceding one, over an orientation range covering both the maximum mass and the minimum mass directions for a material having the simple Fermi ellipsoid of Fig. 18, it would be observed that peaks are "born" in the low-mass direction and "swallowed up" in the high-mass direction. Furthermore, more peaks would be "swallowed" than were being produced (because of the closer spacing in magnetic field of the levels in the high-mass direction) which illustrates why there are fewer peaks in the rotational diagrams at high fields than in the ones at low fields. It should be noted that if the Fermi ellipsoid were made a sphere there would be no peaks in the rotational diagram.

Figure 19 represents the behavior expected for rotation of the magnetic field in the vicinity of an orientation corresponding to an intermediate cyclotron mass. The mass increases continuously, as the magnetic field is rotated from $-\theta$ to $+\theta$. Also, the Landau levels become more closely spaced, the spacing between the peaks decreases and they decrease in height. The effect of increasing the magnetic field is to shift the cooling peaks to the right as is illustrated by the three cooling-peak patterns on the right side of the figure. Each peak will also decrease slowly in height with increasing magnetic field since it is shifting to a higher-mass direction.

If another ellipsoid that is symmetrically related to the one of Fig. 19 is included, the situation is nearly that (except that the high-mass electrons are missing) corresponding to the magnetic field along the binary axis in bismuth. This situation and the corresponding rotational diagrams are illustrated by means of Fig. 20. As the magnetic field is rotated, the cyclotron mass associated with electrons in one of the Fermi ellipsoids increases and that associated with the other one decreases, but they are equivalent at $\theta=0$. Applying the same type of reasoning to this situation as in connection with Figs. 18 and 19 leads to the energy diagram and cooling peak patterns shown. In this case, the cooling peaks associated with one ellipsoid, θ, move to the right with increasing magnetic field and the ones related to the other, θ', move to the left. In the cooling-peak patterns, it is seen that the center peak splits at fields both larger than and smaller than that corresponding to the situation shown for the energy diagram. This splitting of the central peak is different from that of Fig. 18, not only in that it occurs for both increasing and decreasing magnetic field but also in that carriers from two different Fermi ellipsoids are involved in both the high-field and the low-field splitting. In this case, the central peak is an enhanced peak due to the super-

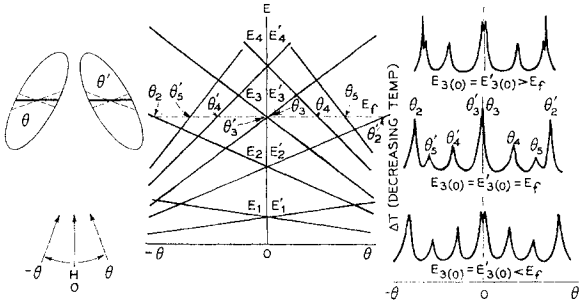

FIG. 20. The effect of the angular dependence of Landau levels on the cooling peak patterns of two symmetrically related Fermi ellipsoids that approximate the situation (except that the high-mass electrons are missing) with the magnetic field along the binary axes of bismuth. The cooling peaks associated with one elliposid, θ, move to the right and those related to the other, θ', move to the left with increasing field. Also, θ_2 and θ_2' move together while each of the pairs, θ_5, θ_5' and θ_4, θ_4', move apart. The central peak at $\theta=0$ splits on either increasing or decreasing the field from the situation represented by the energy diagram and accounts completely for the qualitative behavior of the experimental data shown in Fig. 9.

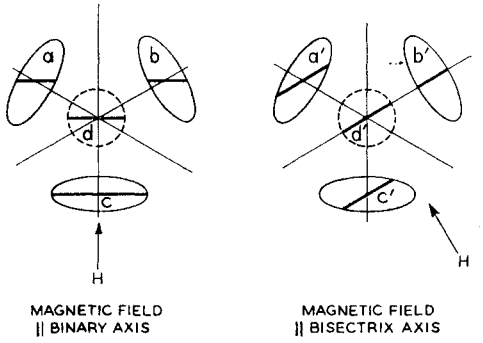

FIG. 21. Simplified schematic representation of the orientation of cyclotron orbits with respect to the constant energy ellipsoids in bismuth. The direction of the magnetic field and planes of cyclotron orbits (heavy lines) are shown for the two symmetry direction cases. In other directions there are four nonequivalent groups of carriers, three of electrons (a, b, and c) and one of holes (d).

position of two peaks when $E_3=E_3'=E_f$. However, these two peaks move in opposite directions with any variation in field and thus separate or split. (See Fig. 9 for an experimental demonstration of this behavior.) In the case represented by Fig. 18, both peaks involved in the splitting are necessarily associated with the same ellipsoid.

It can easily be shown that the two outside peaks θ_2 and θ_2' move toward each other with increasing field, while the pairs θ_5, θ_5' and θ_4, θ_4' move apart. This behavior leads to the formation of the small peaks on the sides of larger peaks (satellites) shown on the upper right of Fig. 20. Further increase of the magnetic field will result in each of these double peaks coalescing into slightly enhanced single peaks as they cross and eventually into small peaks that appear as satellites on the opposite sides of the larger peaks.

Many of the gross features of the observed rotational cooling-peak patterns are similar to those shown in Fig. 20. However, the qualitative features of the observed data can be more easily envisioned with the aid of Fig. 21 which is a simplified representation of the Fermi ellipsoids in bismuth as they appear in the plane of rotation of the magnetic field that was used experimentally.[16]

Since the orientation of each of the four Fermi ellipsoids (a, b, and c=electrons and d=holes) with respect to the magnetic field is different when the field is not in a symmetry direction, four sets of cooling peaks (peak number, p, vs H) are possible (one set from each ellipsoid). However, when the magnetic field is along a symmetry direction (H||binary axis or H||bisectrix axis) the mass of electrons associated with two ellipsoids are identical and the corresponding cooling peaks will coincide to form a single set of double magnitude. Furthermore, in rotational observations, there will be no peaks associated with holes (d) since their cyclotron mass does not change with orientation in this plane.

[16] G. E. Smith, Phys. Rev. **115**, 1561 (1959).

From the above considerations and the arrangement of the ellipsoids shown in Fig. 21, it follows that three series (sets) of peaks are possible when the intensity of the magnetic field is varied while it is along the binary or bisectrix axes. With H along the binary axis, one series should result from ellipsoid c, one from d and one from $a+b$. Likewise, bisectrix series are expected to originate from ellipsoids $a'+c'$, b' and d'. In Figs. 12 and 13 a series of binary peaks associated with low-mass electrons ($a+b$) is shown. The high-mass holes, d, and the high-mass electrons, c, result in two series of peaks too small in magnitude to be resolved in the figures. In Fig. 14, two sets of bisectrix peaks are apparent, originating from b' and $a'+c'$. The lower-mass peaks, b', are superimposed on alternate peaks of the higher-mass series, $a'+c'$. The fact that this particular relationship between the two series of peaks exists means that the cyclotron mass of electrons of ellipsoid b' is almost exactly one-half that of a' and c'.

The various peaks of the observed rotational cooling peak patterns can be correlated with the ellipsoidal scheme of Fig. 21. For example, the bisectrix peak at $+30°$ in Fig. 5 originates from contributions from ellipsoids a', b', and c' of Fig. 21. It is possible to correlate such peaks with the Landau energy levels responsible for their existence.

Spin Splitting

The effect of spin splitting was discussed in the experimental section and is most clearly shown in Fig. 15. The pair of peaks at 14.2 and 15.5 are separated (in $1/H$) by about 8%. However, this is not enough information

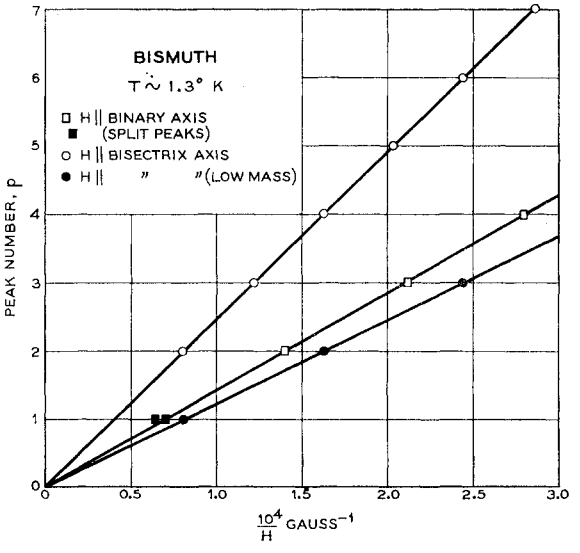

FIG. 22. Peaks numbers vs $1/H$ for three groups of electrons in bismuth. The intercepts of the straight lines are very nearly zero, indicating that the effect of spin splitting is large ($\Delta \lesssim 0.5$). The deviation of the pair of peaks represented by the black squares is attributed to variations of the Fermi energy. The slope of the lines is proportional to m^*E_f of the pertinent groups of carriers.

TABLE II. Comparison of constants for bismuth derived from magnetothermal data with those from cyclotron absorption. The value in parenthesis is taken from the work of Galt *et al.*[17] The letters *a* and *b* do not refer to the Fermi ellipsoid scheme of Fig. 21 but rather to the system used for the subscripts of peak numbers, *p* (*a* refers to lowest mass group of carriers, etc.).

	Magnetothermal	Cyclotron absorption (Galt *et al.*)
Cyclotron masses H‖binary axis		
m_a^*	···	0.13
m_b^*	(0.0105)	0.0105
H‖bisectrix axis		
m_a^*	0.0090	0.0091
m_b^*	0.0180	0.0180
Fermi energy	15.7×10^{-3} eV	···
Fermi temperature	181°K	···

to evaluate Δ since a value of either 0.04 (small amount of spin splitting) or 0.46 (large amount of spin splitting) is consistent with the splitting experimentally observed. In Fig. 22, peak number, p, is plotted against $1/H$ for part of the data of Table I. It is apparent that the intercept is very near zero and thus

$$\Delta_{\text{bin}}=0.46 \tag{7}$$

rather than 0.04. Furthermore, the integral values of the intercepts for high-mass and the low-mass bisectrix peaks show that both of these groups of electrons have large spin splitting ($\Delta\lesssim\frac{1}{2}$).

The fact that the 14.2-kG point representing one of the peaks split by spin falls on the appropriate straight line of Fig. 22, while the 15.5-kG point does not, suggests that the latter peak may be from some entirely different source. This possibility has been considered and is ruled out partly because the splitting is also seen in the 7.4-kG peak in the rotational cooling peak pattern of Fig. 17 and partly because the deviation of the points can be explained in another way. Each time a Landau level passes through the Fermi surface, the Fermi surface is raised slightly and subsequently returns to its average energy. These oscillations in the Fermi energy rapidly become large for low quantum numbers. An estimate of this effect shows that a 4% effect on the last binary peak is reasonable while the effect on the next peak would not be appreciable.

Discussion of Data

Since the Fermi energy does not change with orientation and the slope of the lines of Fig. 22 is proportional to m^*E_f, having a value of E_f or of m^* for some one orientation, makes it possible to evaluate other values directly from the slopes. In Table II, values of m^* for other orientations and a value of E_f have been obtained by using the value of m^* in parenthesis from the work of Galt *et al.*[17] The values of cyclotron masses are in good agreement with those from cyclotron resonance and the Fermi energy is in reasonable agreement with Shoenberg's value [15](Fermi temperature = 205°K).

ACKNOWLEDGMENTS

The authors wish to thank M. Tanenbaum for much encouragement and several stimulating discussions. The assistance of K. F. Rodgers in the preparation of the carbon thermometer, of J. P. Maita with the initial experiments, and of G. F. Brennert with several of the later experiments, is appreciated.

[17] J. K. Galt, W. A. Yager, F. R. Merritt, B. B. Cetlin, and A. D. Brailsford, Phys. Rev. **114**, 1396 (1959).